Tuning the Organogelating and Spectroscopic Properties of a C3-Symmetric Pyrene-Based Gelator through Charge Transfer

Adrian Gainar, Thanh-loan Lai, Cristina Oliveras-González, Flavia Pop, Matthieu Raynal, Benjamin Isare, Laurent Bouteiller, Mathieu Linares, David Canevet, Narcis Avarvari, et al.

Tuning the organogelating and spectroscopic properties of a *C*$_3$-symmetric pyrene-based gelator through charge transfer

Adrian Gainar,[+][a] Thanh-Loan Lai,[+][b] Cristina Oliveras-González,[b] Flavia Pop,[b] Matthieu Raynal,[a] Benjamin Isare,[a] Laurent Bouteiller,*[a] Mathieu Linares,[c] David Canevet,*[b] Narcis Avarvari,*[b] Marc Sallé*[b]

Abstract: Two-component organogels and xerogels based on a *C*$_3$-symmetric pyrene-containing gelator have been deeply characterized through a wide range of techniques. Based on the formation of charge transfer complexes, the gelation phenomenon proved to be highly dependent on the nature of the electron poor dopant. This parameter significantly influenced the corresponding gelation domains, the critical gelation concentrations of acceptor dopants, the gel-to-sol transition temperatures, the microstructures formed in the xerogel state and their spectroscopic properties. In particular, titrations and variable-temperature UV-visible absorption spectroscopy demonstrated the key role of donor-acceptor interactions with a remarkable correlation between the phase transition temperatures and the disappearance of the characteristic charge transfer bands. The assignment of these electronic transitions was confirmed through time-dependent density functional theory (TD-DFT) calculations. Eventually, it was shown that the luminescent properties of these materials can be tuned with the temperature, either in intensity or emission wavelength.

Introduction

Supramolecular gels represent a very important family of soft materials formed through the self-assembly of low molecular weight gelators upon a complex bottom-up process, during which molecules of solvent are entrapped in a network of fibers.[1–3] Applications of organogels and derived xerogels in various fields such as luminescent soft materials,[4–10] sensing,[11–17] organic electronics,[18,19] pharmaceutics,[20–24] photoconductivity[25] have been reported in the last fifteen years. Various polycondensed aromatic functional units such as anthracene,[9] fluorene,[10] tetracene,[26] naphthalene diimide (NDI),[27–29] perylene diimide (PDI),[30–32] hexabenzocoronene (HBC),[6] have been introduced in supramolecular gelators in order to take advantage of their emission and/or redox active character. Electroactive organogels arouse interest as they can reversibly respond to redox stimuli and their gelation properties can thus be modulated.[33,34]

In this respect, a particularly attractive unit is pyrene (Pyr) as it combines both luminescence,[35] redox activity,[36] and straightforward functionalization towards organogelators.[37] It is therefore not surprising that several families of pyrene-based functional organogels have been reported,[38–46] including two-component donor-acceptor (D/A) organogels combining pyrene derivatives with trinitrofluorenone (TNF),[47–50] or porphyrins[51] as electron-acceptors, for example. These two-component organogels show fluorescent properties that constitute a relevant output to probe the Pyr···A interactions taking place upon gel formation.[39,52,53]

The previously reported pyrene-based supramolecular organogelators contain in their structure, beside the pyrene moiety, an organogelating unit able to self-assemble upon non-covalent interactions to generate nanostructures. In this context, appending N-monoacylated 2,2'-bipyridine-3,3'-diamine wedges to a central 1,3,5-benzenetricarbonyl unit[54] generates benzene-1,3,5-tris(3,3'-diamido-2,2'-bipyridine) (BTABP) derivatives, as valuable and versatile building blocks.[55,56] Intramolecular hydrogen bonding imparts BTABP monomers a rigid propeller-shaped conformation, which allows their self-assembly through π-π stacking.[57] Electro- and photoactive BTABP derivatives affording functional gels and supramolecular aggregates have been described with tetrathiafulvalene (TTF)[58–61] and porphyrin substituents.[62,63] The attachment of pyrene units at the periphery of BTABP platform has been recently reported by some of us together with its gel formation ability.[64] Compound **C$_3$Pyr** (Scheme 1) forms gels in 1,1,2,2-tetrachloroethane (TCE) at a critical gelation concentration (CGC)[65] of 65 mg.mL^{-1} (4.26×10^{-2} M). Interestingly, adding three equivalents of tetracyanoquinodimethane (TCNQ) provokes a dramatic

[a] Dr A. Gainar, Dr M. Raynal, Dr B. Isare, Dr L. Bouteiller
Sorbonne Université, CNRS, Institut Parisien de Chimie Moléculaire, Equipe Chimie des Polymères, 4 Place Jussieu, 75005 Paris, France. E-mail: laurent.bouteiller@upmc.fr
[b] Dr T.-L. Lai, Dr C. Oliveras, Dr F. Pop, Dr D. Canevet, Dr N. Avarvari, Pr. M. Sallé
Laboratoire MOLTECH-Anjou
UNIV. Angers, UMR CNRS 6200, SFR MATRIX
2 Bd Lavoisier, 49045 Angers Cedex, France
E-mail: david.canevet@univ-angers.fr, narcis.avarvari@univ-angers.fr, marc.salle@univ-angers.fr
[c] Dr. M. Linares, Laboratory of Organic Electronics and Group of Scientific Visualization, ITN, Linköping University, 60174 Norrköping, Sweden
Swedish e-Science Reseach Center (SeRC), Linkoping University, SE-581 83 Linköping, Sweden
[+] These authors contributed equally to the present work.

Supporting information for this article is given via a link at the end of the document.

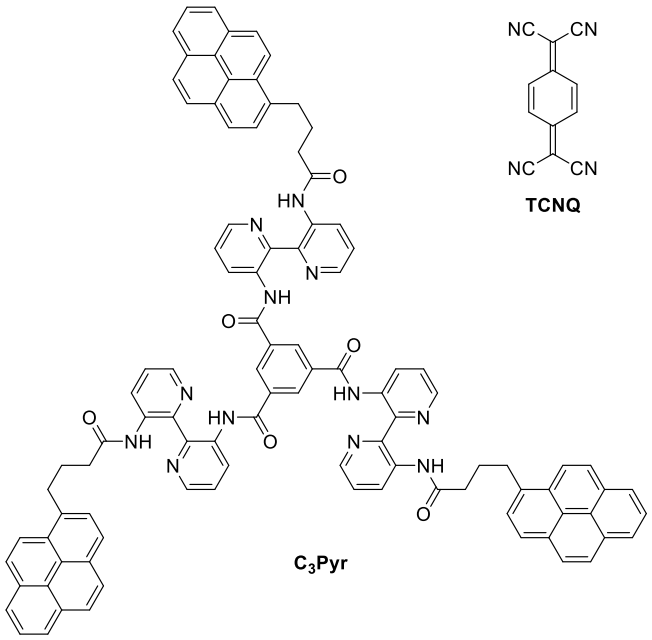

Scheme 1. Chemical structures of **C₃Pyr** and TCNQ.

decrease of the CGC by one order of magnitude (8 mg.mL^{-1}). Thereby, a robust dark brown gel ((TCNQ)$_3$/**C₃Pyr**) formed when the warm solution was subsequently cooled to room temperature, suggesting the involvement of the three pyrene units of **C₃Pyr** in intermolecular donor-acceptor interactions with TCNQ. This was also supported by the appearance of Pyr⋯TCNQ charge transfer (CT) bands in the UV-visible absorption spectra and a {Pyr-TCNQ}* exciplex emission band. This first D-A organogel based on the tris(pyrene) compound **C₃Pyr** paved the way towards the preparation of a whole family of electro- and photoactive two-component gels by using various π-accepting units and motivated further investigations on the mechanism of the process and the key interactions involved in the gel formation. In particular, our approach to prepare two-component functional donor-acceptor organogels and xerogels is highly modular since it allows the use of a large variety of simple acceptor molecules, thus ensuring easy tuning of the gelation behavior and targeted properties. The parallel approach, consisting in the use of both donor and acceptor moieties supported on self-assembly units, has been addressed, for example, by Ajayaghosh *et al.* through the self-sorting of *C₃*-OPV and *C₃*-PDI precursors containing a BTA (benzene-1,3,5-tris(amide) core, providing supercoiled supramolecular ropes showing fluorescence sensing towards aromatic volatile organic compounds (VOCs).[66] However, this approach requires multiple synthetic steps for both components.
We present herein a comprehensive comparative study on the gelation properties of compound **C₃Pyr** in the presence of the series of acceptors TCNQ, tetrafluoro-tetracyanoquinodimethane (TCNQ-F$_4$), naphthalene diimide (NDI) and dicyanomethylene-trinitrofluorene (DCTNF), together with the physico-chemical characteristics of the corresponding gels.

Results and Discussion

Organogelating properties of C₃Pyr.

C₃Pyr proved to gelate chlorobenzene (CB), 1,1,2,2-tetrachloroethane (TCE), 1,2-dichlorobenzene (*o*DCB), and 1,2,4-trichlorobenzene (TCB) (see Figure 1). It shows therefore a good propensity to gelate chlorinated solvents but also tetralin (1,2,3,4-tetrahydronaphthalene). These solvents have in common to display high boiling points, which suggests that strong intermolecular interactions occur between **C₃Pyr** molecules and that high temperatures are required to break the initially formed aggregates. A particular behavior was observed in the case of TCE: 1) unlike other solvents, which afforded suspensions, adding **C₃Pyr** to TCE at concentrations below the CGC afforded homogeneous solutions; 2) while gelation occurred within 30 minutes at a concentration C = 65 mg.mL^{-1}, a particularly slow gelation process was observed (after about a month) when considering samples at concentration C' = 8 mg.mL^{-1} (Figure 1). Representative scanning electron microscopy (SEM) images of the pure **C₃Pyr** xerogels obtained by drop-casting hot solutions at the corresponding CGCs are shown in Figure S1 (SI). In these images, dense networks of intertwined nanofibers can be observed independent from the solvent under consideration. In all cases, these nanofibers proved to assemble into micrometric structures (Figure S1).

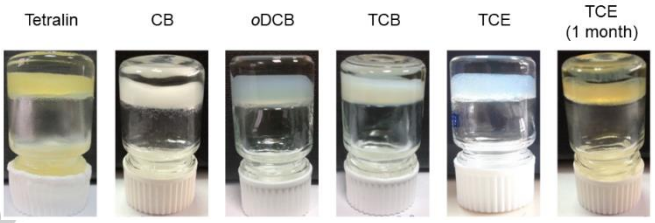

Figure 1. Organogels of **C₃Pyr** from different solvents at the CGC values mentioned in Table 1, and C' = 8 mg.mL^{-1} in TCE for the very right sample obtained after 1 month, respectively (**C₃Pyr** was insoluble in boiling chloroform, tetrahydrofuran, acetonitrile, 1,4-dioxane, toluene, *p*-xylene, dimethylsulfoxide, hexadecane; precipitation in octan-1-ol).

Table 1. Gelation tests for compound **C₃Pyr** (G gel formation). For gels G (x), x is CGC in mg.mL^{-1}, i.e. the required minimum organogelator amount for gel formation at 20 °C, 24 h after cooling the hot solution.

Solvent	Result	b.p. [°C]	Dielectric constant[67]	Dipole moment[67]
CB	G (12)	134	5.7	1.69
TCE	G(65)	146	8.5	1.32
*o*DCB	G (8)	179	10.1	2.5
Tetralin	G (36)	208	2.8	0
TCB	G (29)	214	2.2	1.26

Gelation studies: C_3Pyr in the presence of various acceptors.

Tris(3,3'-diamido-2,2'-bipyridine)-benzene-1,3,5-tricarboxamide-based C_3 compounds exhibit a strong propensity to form highly ordered nanostructures through combined intramolecular H-bonds and intermolecular π-π interactions.[58–64] On the other hand, pyrene is known to interact with electron-poor molecules such as TNF[47–50] and TCNQ.[68,69] The **C_3Pyr** system, bearing three attached donating (D) pyrene groups surrounding the C_3 platform, behaves as an electron-rich supramolecular building block. It appears therefore very appealing to test the ability of electron-poor units (accepting groups A) to interact and to contribute to the nanostructuring process of **C_3Pyr** into D-A organogels.

As mentioned before, we recently demonstrated that the gelation capacity of **C_3Pyr** in TCE increases dramatically upon addition of the π-accepting unit TCNQ, through the establishment of intermolecular D–A interactions.[64] We were interested in rationalizing / extending the scope of this observation by using a broad range of π-accepting molecules.

*Gelation from a fixed concentration of **C_3Pyr** (8 mg.mL^{-1} in TCE) and various (A)/(**C_3Pyr**) ratios.*

Since a relatively high CGC was observed for **C_3Pyr** in TCE (65 mg.mL^{-1}), the experiments were led at a concentration of 8 mg.mL^{-1} in this solvent, avoiding therefore solubility issues along the spectroscopic studies. In addition to the previously studied TCNQ molecule, we addressed the case of other well-established π-accepting molecules, differing either in their geometry (2D vs 3D), in their extended π-conjugation or in their electron-poor character: TCNQ-F_4, NDI, DCTNF, dimethylviologen (DMV), dicyanoquinonediimine (DCNQI), *p*-dicyanobenzene (*p*-DCNB), perylene diimide (PDI), picric acid (PA) or C_{60} (Scheme 2). Remarkably, under those conditions, adding TCNQ, TCNQ-F_4,

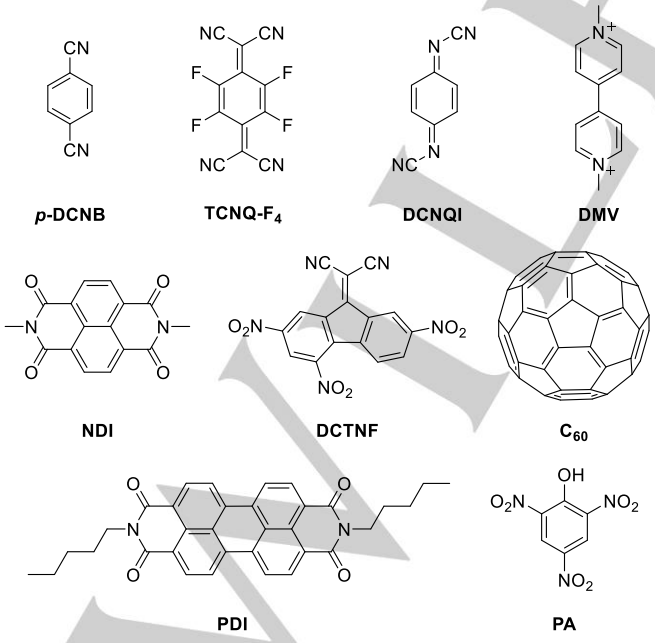

Scheme 2. Chemical structures of the tested acceptors (A)

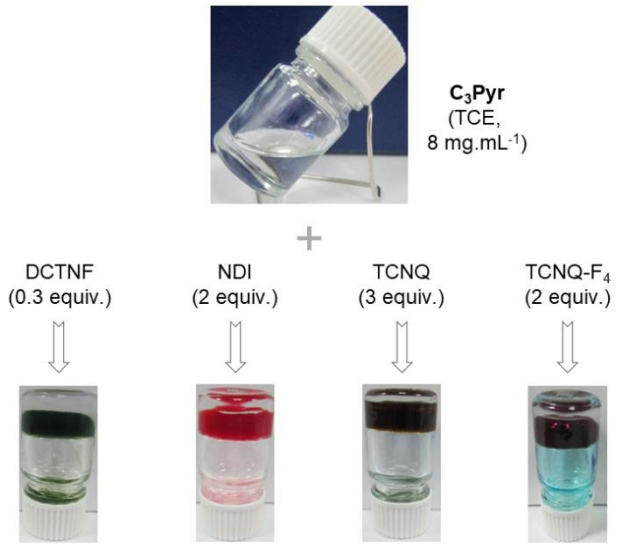

Figure 2. Donor-acceptor two-component organogels, obtained through addition of a minimal amount of a π-accepting molecule to generate a gel from a solution of **C_3Pyr** (8 mg.mL^{-1} in TCE).

NDI or DCTNF to a solution of **C_3Pyr** (8 mg.mL^{-1}) affords robust thermoreversible gels after a heating/cooling sequence (Figure 2). The resulting gels possess an intense color, which is strong evidence of a CT interaction occurring between the donor and acceptor counterparts. Importantly, the minimum amount to reach gel formation is not the same for each of the studied π-accepting molecule. Indeed, three equivalents of TCNQ are required to form a robust dark brown gel from **C_3Pyr** (8 mg.mL^{-1} in TCE). This result suggests the involvement of all pyrene units in donor-acceptor interactions and thus the formation of alternate D-A stacks within the nanostructure. Remarkably, the required minimum amount decreases for the other acceptors to a value as low as 0.3 molecular equivalent in the case of DCTNF, which suggests a different organization in this case.

Conversely, it is worth noting that gel formation could not be observed upon adding alternative electron-poor units such as the π-conjugated DMV, DCNQI, or PA units or the three-dimensional C_{60} fullerene. These observations do confirm that a good combination of specific electronic and geometric conditions are required in order to promote a gel formation driven by D-A interactions. For instance, if a D-A-D-A alternating mixed stack is presumed to guide the growth process through intercalation between the **C_3Pyr** molecules, it is rather intuitive to consider that the 3D C_{60} molecule, albeit electron accepting, is geometrically inappropriate, and that planar electron-poor derivatives are more suitable. Considering the electronic properties, an immediate comparison of the respective electron-poor character of the acceptor molecules can be implemented from cyclic voltammetry experiments (Figure S2). According to this study, we were able to rank these units along their π-accepting character: TCNQ-F_4 > TCNQ > DCTNF > NDI. Therefore, this parameter alone cannot justify the higher propensity of DCTNF among those molecules to promote gelation in TCE, and other geometrical parameters need

to be considered (*e.g.* size, symmetry, extension of the conjugated π-system).

In order to assess the impact of the acceptors on the gel phase behavior, the gel-solution transition temperatures ($T_{g\text{-}s}$) of the D-A composites were determined according to the "falling-ball" method.[70] In the presence of three equivalents of the different acceptors, the $T_{g\text{-}s}$ values proved to vary from 40 °C (313 K, TCNQ) to 130 °C (403 K, DCTNF) (Figure 3). Noteworthy, the acceptors that respectively provide the lowest and the highest $T_{g\text{-}s}$ are the ones requiring the largest and the smallest amounts to afford gels. To gain more insight on this feature, systematic measurements of $T_{g\text{-}s}$ were led with various A/**C₃Pyr** ratios. Two distinctive behaviors can be distinguished from Figure 3. In the case of the strongly π-accepting TCNQ and TCNQ-F_4 molecules, the $T_{g\text{-}s}$ first dramatically increases with the (A)/(**C₃Pyr**) ratio and then rapidly reaches a plateau value (333 K and 363 K, respectively). The corresponding plateau is reached for 3 to 4 equivalents of added A compound. Given the fact that **C₃Pyr** involves three pyrene units, this observation is reminiscent of an alternating -D-A-D-A- organization within the gel nanostructure. In the case of the DCTNF and NDI derivatives, which present a significantly larger π-extension (Figure S3), a different scheme arises. In those cases, a steady increase of the $T_{g\text{-}s}$ is observed within the temperature range under study, without reaching any plateau value (note that higher (A)/(**C₃Pyr**) ratios could not be reached due to precipitation). From this study, it appears that the gel-solution transition temperatures ($T_{g\text{-}s}$) of the D-A composites strongly depend on the (A)/(**C₃Pyr**) ratio. For instance, shifting from 0.3 equivalent of DCTNF to 3 equivalents allows a spectacular increase of 55 °C of the $T_{g\text{-}s}$ (from 343 to 398 K). One can note in addition, the remarkably high $T_{g\text{-}s}$ values observed in the case of DCTNF (>70 °C), even for very low amounts of introduced A molecule, illustrating a specifically high stability for this two-component organogel.

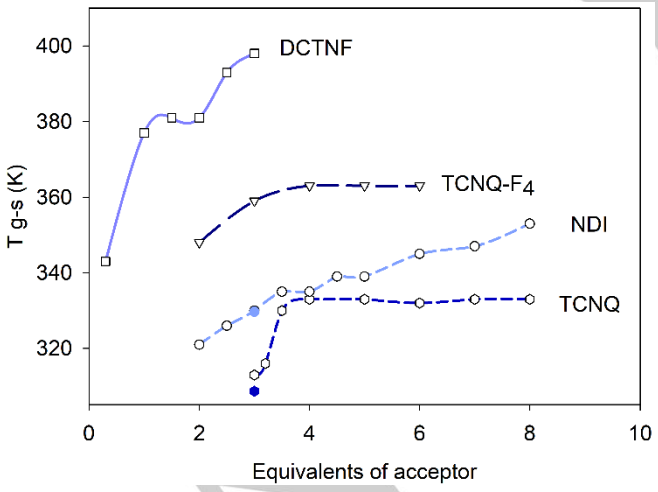

Figure 3. Evolution of the gel-sol transition temperature ($T_{g\text{-}s}$) as a function of the (**A**)/(**C₃Pyr**) ratio ([**C₃Pyr**] = 8 mg.mL^{-1} in TCE) for various **A** compounds. Hollow symbols correspond to the falling ball method. Filled symbols correspond to $T_{g\text{-}s}$ values determined by nanoDSC technique in the presence of three equivalents of NDI or TCNQ.

*CGCs in TCE for a fixed (A)/(**C₃Pyr**) ratio 3/1 (A = DCTNF, TCNQ-F_4, NDI, TCNQ)*

As shown above, the (A)/(**C₃Pyr**) ratio appears critical regarding the respective gelation properties and gel characteristics. In a complementary manner, the CGCs of these two-component organogels constitute relevant parameters. In order to compare the behavior of the different two-component D-A organogels, we carried out a dilution study using a systematic $(A)_3/(\mathbf{C_3Pyr})_1$ ratio (Figure 4). Those gelation tests were conducted by following a simple heating-cooling sequence. The starting solution contains a concentration of 8 mg.mL^{-1} **C₃Pyr** in TCE, in which a threefold stoichiometry of the A compound was added. Using this (A)/(**C₃Pyr**) ratio, a gel state is reached whatever the acceptor, thus confirming the positive effect of the CT over the gelation process (CGC = 65 mg.mL^{-1} for **C₃Pyr** alone). Successive dilutions of the $(A)_3/(\mathbf{C_3Pyr})_1$ mixtures were then operated in order to assess the concentration effect over the gelation capability of the mixture.

Again, the case of the DCTNF acceptor seems particularly appealing since this acceptor drives gelation for a concentration as low as 1 mg.mL^{-1} in **C₃Pyr**. As such, the **C₃Pyr**/DCTNF combination constitutes a rare example of two-component supergelator based on charge transfer interaction.[71,72]

In order to study these D-A two-component organogels in a quantitative manner, nanoDSC studies were run for the above composites. The samples were studied as gels of $(\mathbf{A})_3/(\mathbf{C_3Pyr})_1$ stoichiometry and prepared from a [**C₃Pyr**] = 8 mg.mL^{-1} concentration in TCE.

Under these conditions, no phase transition could be detected through this technique with **C₃Pyr** alone (Figure S4), which appears reasonable for a solution, as well as for $(\mathbf{TCNQ\text{-}F_4})_3/(\mathbf{C_3Pyr})_1$ and $(\mathbf{DCTNF})_3/(\mathbf{C_3Pyr})_1$ mixtures (Figure S5). This most likely results from their higher $T_{g\text{-}s}$, which makes difficult the insertion of the gel in the nanoDSC capillary, since signals were detected with NDI and TCNQ. In both cases, broad endothermal events are detected upon heating with maxima at 57°C (NDI, 330 K, Figure 5) and 36°C (TCNQ, 309 K, Figure S6), which coincides with the values determined through the 'falling-ball' method (Figure 3). Upon cooling, exothermal events are respectively detected at temperatures 20°C lower than in the heating processes, which is a classical signature of a nucleated self-assembly.[73] Interestingly, the heating and cooling curves of subsequent cycles are perfectly superimposed showing the

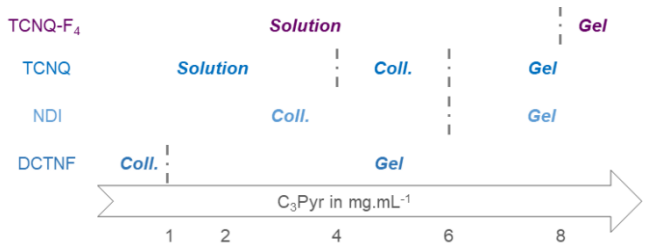

Figure 4. Gelation domains using a $(A)_3/(\mathbf{C_3Pyr})_1$ stoichiometry at various concentrations in TCE. 'Coll.' stands for colloidal dispersion.

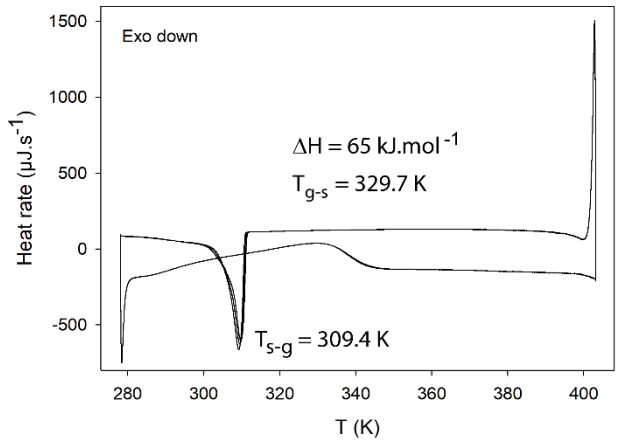

Figure 5. DSC Thermogram recorded for a $(NDI)_3$(**C_3Pyr**)$_1$ sample in TCE (v = 2 K.min^{-1}). [**C_3Pyr**] = 8 mg.mL^{-1}.

reversibility of the process and the absence of thermal degradation up to 130°C. Eventually, it appears worth noting that the enthalpies associated to the sol-gel transitions are similar for $(TCNQ)_3$/(**C_3Pyr**)$_1$ and $(NDI)_3$/(**C_3Pyr**)$_1$ organogels (65 kJ per mol of **C_3Pyr**).

Microscopic analyses of xerogels

Optical microscopy

In order to assess the influence of the acceptor on the microstructures formed in the xerogel state, *i.e.* after evaporation of the solvent from the gel, optical microscopy constitutes a first valuable tool. Thus, optical micrographs of the different xerogels were recorded under non-polarized and polarized lights (Figures 6 and S7a). Whatever the acceptor under consideration, these images show evidence of the fibrillar structures responsible for the organogelating properties. Moreover, these fibers display birefringence, as demonstrated by polarized-light optical microscopy. Consequently, they display a certain degree of organization at the mesoscopic scale, as expected from such self-assembled materials.

Scanning Electron Microscopy (SEM)

SEM Microscopy represents a complementary and powerful technique to study xerogel materials. In particular, it allows measuring the dimensions of the micro and nano-objects composing the material. To perform such analyses on xerogels, hot solutions of **C_3Pyr** (8 mg.mL^{-1}) and acceptors (3 equiv.) in TCE were drop-casted over aluminium stubs. For each of the four systems, as well as for **C_3Pyr** alone (same experimental conditions), a mesh of entwined micrometer-sized well-defined fibers with diameters comprised between 20 and 30 nm was observed (Figure 7). The dimensions of these fibers compare very well with fibrillar assemblies of other BTABP molecules reported in the literature.[58] Based on theoretical calculations (see § Molecular modelling), these diameters appear consistent with bundles including between five and seven molecules in their cross section.

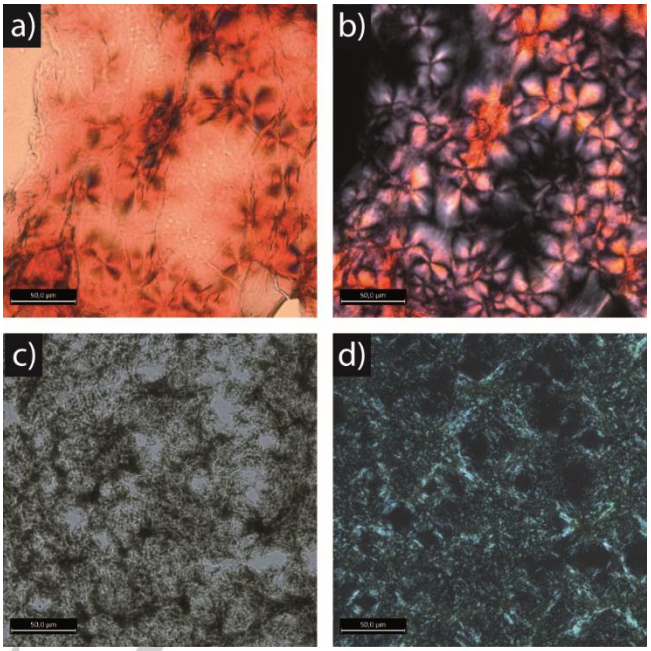

Figure 6. *Top.* Optical micrographs of a $(NDI)_3$(**C_3Pyr**)$_1$ xerogel under non-polarized (a) and polarized (b) lights. *Bottom*. Optical micrographs of a $(TCNQ\text{-}F_4)_3$(**C_3Pyr**)$_1$ xerogel under non-polarized (c) and polarized (d) lights. The images correspond to the same area.

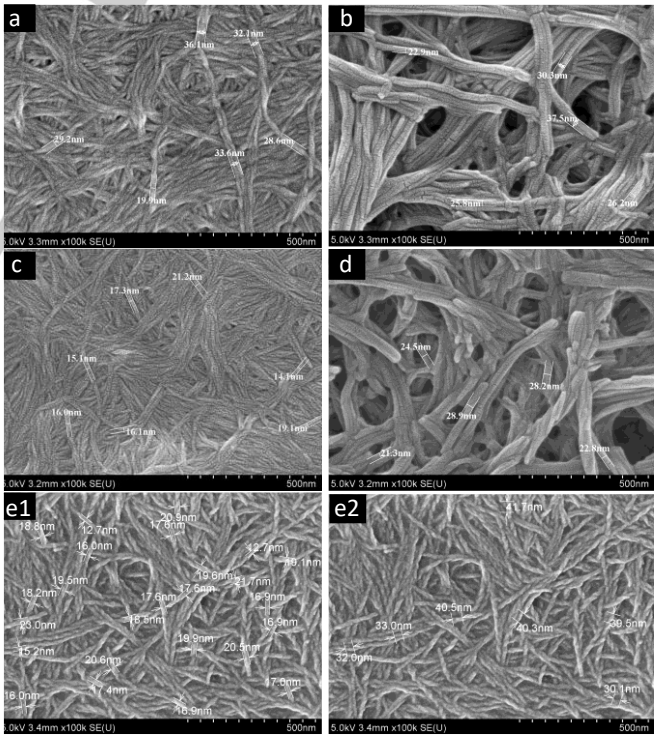

Figure 7. SEM images of xerogels obtained by drop-casting hot solutions of **C_3Pyr** (8 mg.mL^{-1}) in the presence (3 equiv.) of a) TCNQ, b) $TCNQ\text{-}F_4$, c) NDI, d) DCTNF or e) in their absence. While fiber diameters are illustrated in picture a-e1, helical pitches are shown in e2.

The influence of the acceptor on the structure of the fibers can be clearly inferred from the different aspect of the fibers formed out of **C$_3$Pyr** alone at the same concentration. Contrary to **C$_3$Pyr**/**A** bi-component xerogels, fibers of **C$_3$Pyr** alone show a helical structure, both helicities being present as no chiral bias was involved in the gel formation. This observation encouraged us to perform X-ray powder diffraction analyses on these samples (Figure S7b). Nevertheless, these bicomponent xerogels display featureless and similar diffractograms, which likely result from a lack of crystallinity.

Spectroscopic properties

Infrared absorption spectroscopy

Infrared (IR) absorption spectroscopy has been widely used to estimate the degree of charge transfer (DCT) in **D**-**A** complexes involving the TCNQ unit.[68,74,75] A correlation can be drawn between the vibration frequency of its cyano (CN) groups and the DCT, limit reference compounds being neutral TCNQ (ρ = 0 e$^-$ / molecule) and the salt TCNQ-K (ρ = 1 e$^-$ / molecule). Considering the (TCNQ)$_3$/(**C$_3$Pyr**)$_1$ xerogels, IR spectroscopy confirmed the occurrence of a CT, as shown by the wavenumber of the CN transition (2218 cm^{-1} – Table 2, Figures S8 and S9a).

Table 2. IR vibration frequencies of various acceptors A, together with their corresponding shifted values of (A)$_3$/(**C$_3$Pyr**)$_1$ CT complexes measured in solid-state.

A	ν_{CN} A [cm^{-1}]	ν_{CN} (A)$_3$/(C$_3$-Pyr)$_1$ [cm^{-1}]
TCNQ	2223	2218
TCNQ-F$_4$	2227	2217
DCTNF	2230	2227

This constitutes an important information since it demonstrates that TCNQ does interact with pyrene in the xerogel state and is embedded within the microstructures, with a DCT of *ca.* 0.14 e$^-$ / molecule according to the linear correlation between DCT and the wavenumber of the CN band.[74] Similar results were obtained for (TCNQ-F$_4$)$_3$/(**C$_3$Pyr**)$_1$ (2217 cm^{-1}, Table 2, Figures S8 and S9b) with a higher DCT (ca. 0.31 e$^-$ per molecule),[76–78] and for (DCTNF)$_3$/(**C$_3$Pyr**)$_1$ (2227 cm^{-1}, Table 2, Figures S8 and S9c) with a lower DCT (ca. 0.07 e$^-$/molecule)[79] respectively to (TCNQ)$_3$/(**C$_3$Pyr**)$_1$, which is in line with the π-accepting character of each acceptor unit (*vide supra*).

^{1}H NMR spectroscopy

In order to gain insight on the interactions occurring between the different components and the co-assembly pattern along the supramolecular fibers, the **A**/**C$_3$Pyr** mixtures were studied by ^{1}H NMR spectroscopy. For this purpose, samples containing **C$_3$Pyr** (8 mg.mL^{-1}, 5.24 × 10^{-3} mol.L^{-1}) and 3 equivalents of acceptor (1.57 × 10^{-2} mol.L^{-1}) were first analyzed in 1,1,2,2-tetrachloroethane-d$_2$ (TCE-d$_2$) at 293 K (Figures S10-S13). In the cases of DCTNF, NDI and TCNQ, the signals of the free acceptors were no longer observable (Figures S10-S13), which confirms their interaction with **C$_3$Pyr**. Regarding the latter, moderate variations were detected upon introducing the electron-poor additives. For instance, the chemical shift of the internal NH signal was shifted from 15.26 ppm by $\Delta\delta$ = + 0.09 (DCTNF), + 0.07 (NDI), and + 0.01 (TCNQ) (Figures S10-13). Depending on the nature of the π-accepting derivative, moderate to strong variations in intensity were evidenced for a same number of scans. This shows that the concentrations of **C$_3$Pyr** solute decreases when adding the acceptors and hence, that **C$_3$Pyr** is involved into supramolecular assemblies that are no longer in solution. Consequently, these ^{1}H NMR spectra correspond to the remaining part of **C$_3$Pyr** in TCE-d$_2$, which correlates well with the rather moderate variations of the associated chemical shifts. In order to confirm this assertion, variable-temperature NMR experiments constitute a relevant tool, since it represents a way to accelerate the dynamics of a given equilibrium and shift its position. Thereby, such experiments were led in the absence (Figure S14) or the presence of acceptors and are presented in Figures 8 and S15-S19. Independent from the acceptor under consideration, heating the samples led to increased intensities, higher resolutions and progressive upfield shifts of both NH protons located at 13.7 and 15.3 ppm at room temperature. A sharpening of the NDI (ca 8.7 ppm, Figure S15), TCNQ (7.5 ppm, Figures S16 and S17) and TCNQ-F$_4$ (see Figures S18 and 19) signals was also observed. Moreover, these experiments evidenced a moderate deshielding of the acceptor signals, which appears reasonable since donor-acceptor pairs are weakened upon heating. Given the specific and remarkably strong propensity of **C$_3$Pyr** to generate a gel in the presence of DCTNF (0.3 equiv.) in TCE, we carried out additional ^{1}H NMR analyses of this binary mixture (Figures 9 and S20). In this manner, NMR peaks of DCTNF are absent and those of **C$_3$Pyr** have lower intensity in this mixture relatively to the same peaks in their individuals solutions. At this stage, one will also note that no evolution of the recorded signal intensities was detected over 90 minutes, showing the steady state of the aggregates. On the other hand, introducing a tiny excess of DCTNF acceptor (3 equiv. + ε) results in the complete suppression of the **C$_3$Pyr** signals and the emergence of new peaks corresponding to the excess of DCTNF (Figure 9). This underlines the fact that **C$_3$Pyr** is fully involved into non-detectable aggregates in these conditions. Moreover, this

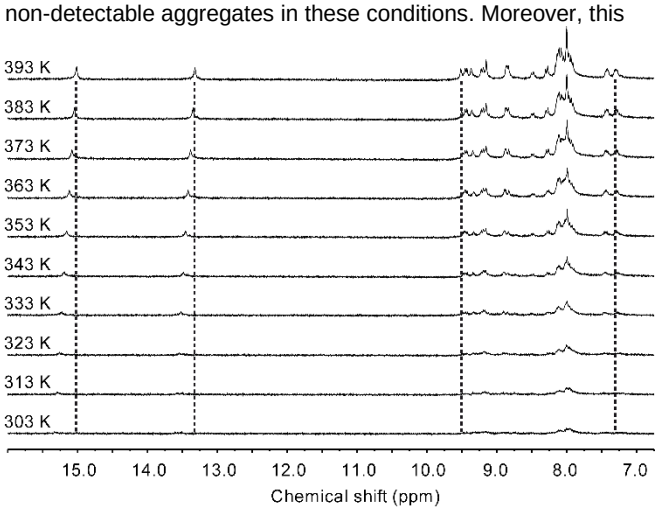

Figure 8. Evolution of the ^{1}H NMR spectrum of a mixture of **C$_3$Pyr** (8 mg.mL^{-1}) and DCTNF (3 equiv.) in TCE upon cooling.

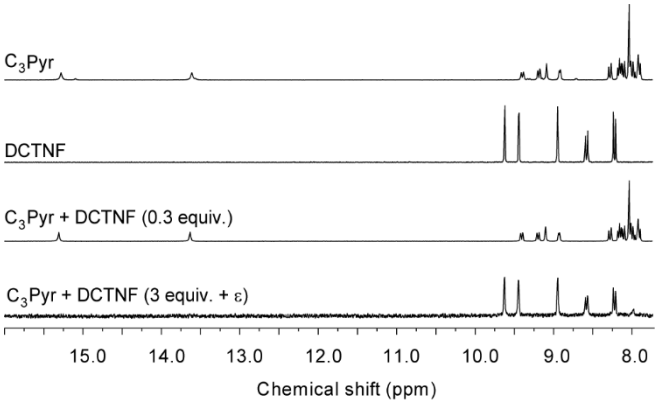

Figure 9. ^{1}H NMR spectra of **C₃Pyr** (8 mg.mL^{-1}), DCTNF and their mixtures (0.3 or 3 equiv. of acceptor) in TCE-d_2.

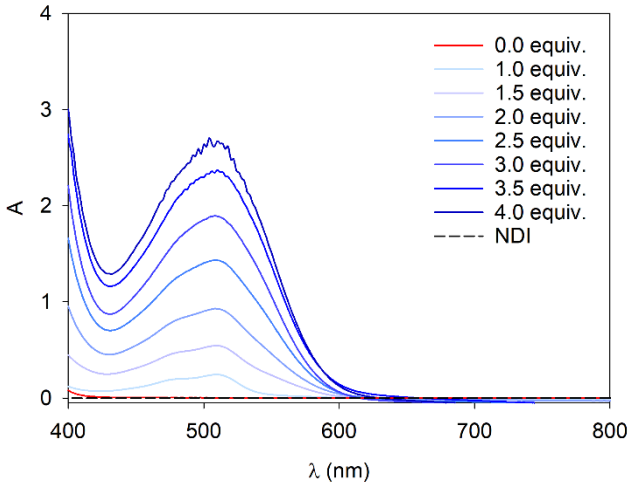

Figure 10. Evolution of the UV-visible absorption spectrum of **C₃Pyr** (8 mg.mL^{-1}, 5.2 mM in TCE, 293 K) upon addition of NDI acceptor. The scattering was corrected by subtracting the absorbance at 800 nm.

experiment shows that the chemical shifts of the excess DCTNF are identical to its free form. Consequently, this excess does not interact with pyrene units and remains in solution.

UV-visible absorption spectroscopy

As mentioned above, adding the acceptors onto **C₃Pyr** solutions results in strong color changes. To characterize the transitions responsible for this phenomenon, UV-visible absorption spectra of **C₃Pyr** donor, acceptors and their respective mixtures were recorded ([**C₃Pyr**] = 8 mg.mL^{-1}, TCE, r.t., Figure S21). In this manner, clear charge transfer bands appeared with DCTNF (λ_{max} = 664 nm), NDI (λ_{max} = 508 nm), TCNQ (λ_{max} = 780 nm) and TCNQ-F_4 (λ_{max} = 564, 752 nm). Titrations were led with the different acceptors in order to get information regarding these CT complexes. These experiments were carried out on **C₃Pyr** solutions (8 mg.mL^{-1} in TCE) from which gels can be obtained in all four cases (Figures 10 and S22-25). A progressive emergence of the CT absorption bands takes place upon increasing the acceptor concentration (Figures 10 and S22-25), without reaching any plateau in the solubility domains of the acceptors.

Along the heating-cooling sequences, we observed a color fading of the samples at high temperatures and the typical color of CT complexes at room temperature. This phenomenon prompted us to perform further analyses to follow the evolution of the CT bands as a function of temperature (Figures 11 and S26-S28). For all acceptors, heating samples containing **C₃Pyr** (8 mg.mL^{-1} in TCE) in the presence of the acceptors (3 equiv.) led to the suppression of the CT bands.[47] Thus, the non-covalent character of donor-acceptor interactions results in materials, whose color and gelating properties are thermally controlled. With this in mind, we compared the gel-to-sol transition temperatures $T_{g\text{-}s}$ determined according to the “falling ball method” and the melting temperatures T_m determined by variable-temperature UV-visible absorption spectroscopy (Figures S26-28), by analogy with the case of proteins. Independent from the nature of the acceptor under consideration, the $T_{g\text{-}s}$ and T_m temperatures proved to be comparable (DCTNF: $T_{g\text{-}s}$ = 398 K; T_m = 369 K; NDI: $T_{g\text{-}s}$ = 330 K; T_m = 326 K; TCNQ: $T_{g\text{-}s}$ = 313 K; T_m = 309 K; TCNQ-F_4:

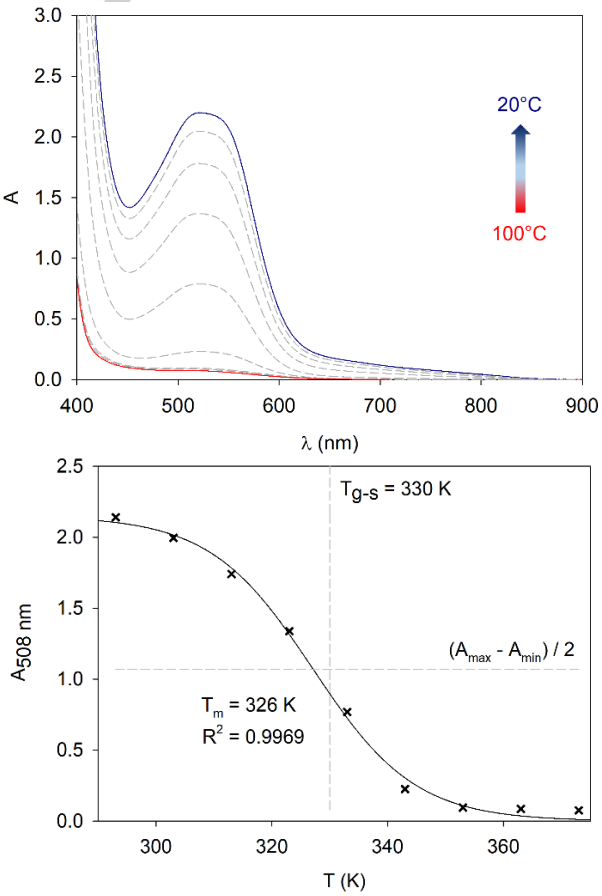

Figure 11. *Top.* Evolution of the UV-visible absorption spectrum of a sample of **C₃Pyr** (8 mg.mL^{-1}) and NDI (3 equiv.) in TCE as a function of temperature (interval of 10 K between each curve – the contribution of scattering was subtracted). Bottom. Corresponding evolution of the absorbance at 508 nm as a function of temperature.

$T_{g\text{-}s}$ = 359 K; T_m = 343 K). One will note that larger differences between T_m and $T_{g\text{-}s}$ values are found for DCTNF and TCNQ-F_4, *i.e.* acceptors that are responsible for high gel-to-sol transition temperatures. In these cases, reaching higher temperatures along the VT spectroscopy experiments was technically not possible and not to be desired regarding safety conditions. This affects the data and most likely leads to underestimated T_m values. On the other hand, the samples containing **C_3Pyr** and the TCNQ or NDI acceptors displayed very similar $T_{g\text{-}s}$ and T_m values. This observation demonstrates and highlights to which extent donor-acceptor interactions are critical to promote the gel-state and tune its physical and spectroscopic properties.

Molecular modelling

In order to have a deeper insight on the association mode of the pyrene donor with the acceptors, DFT calculations have been performed on a model D-A system composed of one pyrene and one TCNQ molecule. As clearly seen in Figure 12, the relative orientation of the two π-units is of paramount importance for the establishment of a charge transfer band. Indeed, for a staggered conformation, reminiscent of the one observed in the crystal structure of pyrene-TCNQ 1:1 complex,[80] two CT bands arising at approx. 500 and 750 nm, very close to the experimentally reported values in pyrene-TCNQ[69] and **C_3Pyr**-TCNQ,[64] are clearly observed. However, such bands are not observed for the eclipsed conformation. To further analyze the effect of the acceptor introduction on the **C_3Pyr**-based complex, a supramolecular assembly formed with **C_3Pyr** and three TCNQ molecules in interaction with the pyrene units was studied (Figure 13). As for the model system, we can see in the complex the formation of a CT band around 770 nm. This band is actually composed of three degenerated electronic transitions (1.61 eV) each corresponding to the excitation of an electron from the pyrene unit to the TCNQ one in front of it. This can clearly be seen by looking at the Natural Transition Orbital[81] provided in Figure S29 for one of the three transitions where the hole is clearly localized on the pyrene unit while the electron is transferred to the TCNQ molecule.

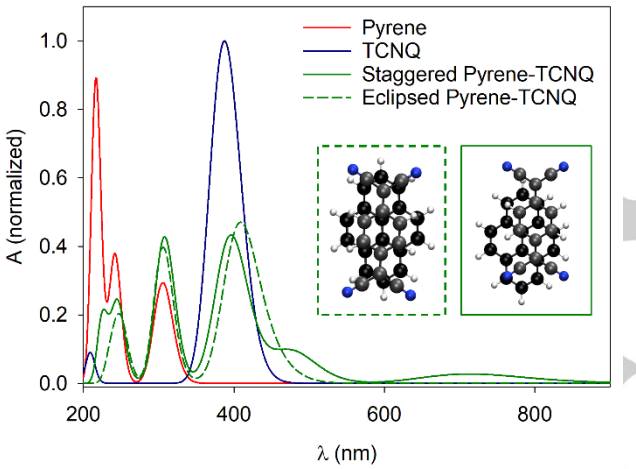

Figure 12. Theoretical UV-visible absorption spectra of the pyrene-TCNQ charge transfer complex for two different relative orientations.

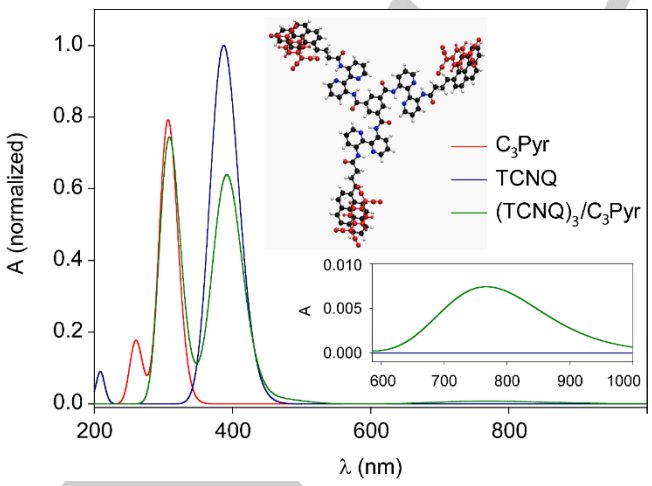

Figure 13. Theoretical UV-visible absorption spectra of the $(TCNQ)_3$/**C_3Pyr** charge transfer complex. Inset: Zoom on the charge transfer band.

Fluorescence spectroscopy

Some of us have reported the original spectroscopic behaviour of **C_3Pyr**,[64] especially in the presence of the TCNQ acceptor. When a solution of **C_3Pyr** in TCE is excited at 344 nm (λ_{max}(pyrene)), a single emission band centered at 515 nm is observed, which corresponds to the radiative relaxation of the tris(bipyridyl) core. In other words, an energy transfer from pyrene to bipyridine units occurs. Upon addition of TCNQ, the situation drastically changed with the appearance of a new emission band (λ_{em} = 580 nm), which could result from the formation of pyrene-TCNQ exciplex. These results encouraged us to assess the influence of various acceptors over the fluorescent properties of the **C_3Pyr** gelator. In order to preserve the thermoreversible features of the corresponding gels, these studies were led in the presence of the critical amount of acceptor required to obtain organogels ([**C_3Pyr**] = 8 mg.mL^{-1}, TCE, 298 K), *i.e.* 0.3 equivalent for DCTNF and 2 equivalents for TCNQ-F_4 and NDI.

In the case of TCNQ-F_4 and upon excitation at 344 nm, the emission intensity increased upon heating the samples (Figure 14), as in the case of TCNQ.[64] Nevertheless, the spectroscopic behaviour significantly differs, since no additional emission band appeared whatever the temperature under consideration. Exciting the solutions at 405 nm allowed the observation of an emission band centered at 570 nm (Figure S30), which increases upon heating and most likely corresponds to the radiative decay of free TCNQ-F_4. This hypothesis was further confirmed by measuring the emission spectra of TCNQ-F_4 at high temperatures (90°C, Figure S30), which perfectly matches the one from the **C_3Pyr** and TCNQ-F_4 mixture. Such a clear conclusion could not be drawn by studying DCTNF-**C_3Pyr** mixtures since both compounds display similar and broad emission spectra (see Figure S31). On the other hand, the spectral modifications observed by mixing **C_3Pyr** with NDI turned out to be significant, as illustrated by Figure 15. Be they excited at 344, 405 or 510 nm (Figure 15 and S32), these

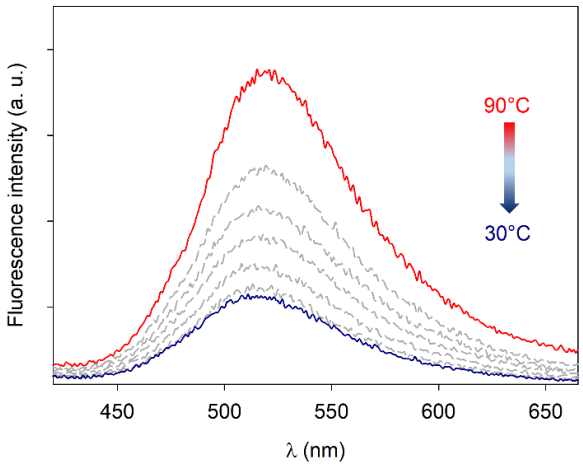

Figure 14. Evolution of the emission spectrum of a **C₃Pyr**-TCNQ-F₄ (3 equiv.) mixture as a function of temperature ([**C₃Pyr**] = 8 mg.mL^{-1}, TCE, λ_{exc} = 344 nm; interval of 10 K between each curve).

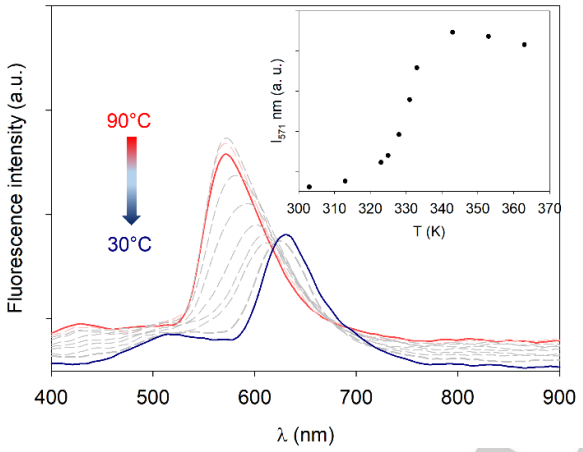

Figure 15. Evolution of the emission spectrum of a **C₃Pyr**-NDI (3 equiv.) mixture as a function of temperature ([**C₃Pyr**] = 8 mg.mL^{-1}, TCE, λ_{exc} = 344 nm). Inset: Corresponding evolution of the emission intensity at 571 nm as a function of temperature.

samples display an emission band centered at 630 nm at room temperature, that is, in the gel state. Upon cooling the samples, this emission band progressively disappears to the benefit of a new bathochromically shifted one (λ_{em} = *ca* 560 nm). Moreover, one will note that an additional emission band (λ_{em} = 450 nm) appears when heating upon excitation at 405 nm (Figure S32). These observations suggest that different species are emitting according to the temperature. In order to gain insight into this behavior, excitation spectra (λ_{em1} = 560 nm and λ_{em2} = 630 nm (Figure S33)) were recorded at various temperatures. These experiments showed that both emissions arise from species that absorb light from 400 to 600 nm. This is the reason why additional measurements were led with pyrene (Pyr) and naphthalene diimide (NDI) serving as references under similar conditions (Figures S34). At high temperatures, the **C₃Pyr**-NDI mixture displays a maximum emission wavelength at 570 nm, which perfectly corresponds to the emission band of NDI in the same conditions. This appears reasonable since the charge transfer complexes constitute thermosensitive species (see UV-visible absorption spectroscopy – Figure 11). More importantly, similar experiments conducted at lower temperature (303 K), *i.e.* in the aggregated state of **C₃Pyr**, show an emission band centered at *ca.* 630 nm, which is not observed for Pyr and NDI references or their mixture (Figure S34). Thus, the presence of the *C₃*-symmetric core of **C₃Pyr** favors the formation of other excited species. Given the poor resolution of this emission band and the significantly larger emission wavelengths in comparison to pyrene-pyrene[35] or NDI-NDI[82] excimers, this emission band is likely to result from the formation of exciplexes between **C₃Pyr** pyrene units and NDI. To our knowledge, this constitutes an unprecedented observation.

Conclusions

As previously reported, the **C₃Pyr** derivative displays moderate organogelating properties that can be improved upon addition of TCNQ acceptor. In this work, we have demonstrated that other electron poor additives, namely TCNQ-F$_4$, DCTNF and NDI, also enhance this gelating ability (Figure 16). A clear impact of the acceptor amount on the gel-sol transition temperatures was evidenced, with variations ranging from 20 K (TCNQ) to 55 K (DCTNF). These variations were definitely linked to structural modifications of the supramolecular fibers, as demonstrated by SEM microscopy. In particular, the helical character of the pure **C₃Pyr** fibers appeared to be lost upon addition of electron-withdrawing additives. ^{1}H NMR analyses also proved valuable since they showed the equilibria between free and bound (frozen) species, be they acceptors or donor **C₃Pyr**, with the progressive disappearance of the signals upon addition of acceptor aliquots. The formation of these species could be followed by naked eye and the colors of the gels could be tuned according to the introduced acceptor. In this regard, UV-visible absorption spectroscopy also constituted an interesting tool to study these supramolecular objects, since this technique allowed highlighting the thermoreversible character of the D-A interactions under consideration.

Given the singular fluorescent properties of pyrene, the impact of the acceptor over the gel luminescence was also investigated. Using TCNQ-F$_4$ as an additive produced gels that do not display any exciplex emission. Therefore, these materials display completely different emission properties in comparison to TCNQ-based ones, despite a similar chemical structure. As far as fluorescence properties are concerned, NDI- **C₃Pyr** organogels constitute a rare example of thermosensitive gel-based materials

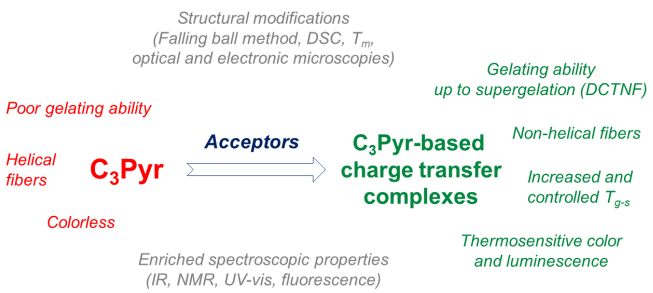

Figure 16. Graphical highlight of the work presented herein.

for which the emission color can be tuned by simple heating or cooling. Eventually, the case of DCTNF-containing gels appears remarkable. Ongoing work involves in-depth rheological studies to understand the role of DCTNF and other acceptors along the supramolecular polymerization process.

Experimental Section

Voltammetric analyses

Cyclovoltammograms were recorded with a EG&G PAR 273 potentiostat. The analyte (10^{-3} mol.L^{-1}) and tetrabutylammonium hexafluorophosphate (Bu_4NPF_6, 0.1 mol.L^{-1}) were dissolved in TCE. The electrochemical cell was equipped with a platinum wire (counter-electrode), a disk-shaped platinum electrode (working electrode, Ø = 2 mm) and a $Ag/AgNO_3$ reference.

TGA and DSC

The **C_3Pyr** xerogel used for TGA and DSC was obtained from filtration of a 32 mg.mL^{-1} gel sample of **C_3Pyr** in TCE. The TCNQ, TCNQ-F_4, NDI and DCTNF acceptors used for DSC and TGA were used as commercially supplied. TGA curves were recorded on a Q50 TA Instruments thermogravimetric analyzer at 5°C.min^{-1}. DSC thermograms were obtained using a Q2000 TA Instruments calorimeter at 5°C.min^{-1} using three consecutive heating-cooling cycles. All samples were measured under N_2 gas flow (50 mL/min). Each experiment was conducted three times (excluding the first heating-cooling cycle used for erasing the thermal history of the sample) to check reproducibility of the experiment. Data treatment was performed using the TA Universal Analysis 2000 software.

NanoDSC

The samples were introduced in solution state into the capillary cell of a N-DSCIII TA Instruments microcalorimeter. The reference cell was filled with pure TCE and the sample cell filled with 0.3 mL of sample solution (including $(A)_3/(\mathbf{C_3Pyr})_1$ in TCE samples, which were left to turn into a gel while inside the capillary before the measurements). The capillary cells were not capped, and a constant pressure of 5×10^5 Pa was applied. Thermograms were acquired in the range 5–130°C at a rate of 1 or 2°C.min^{-1}. Each experiment was conducted three times (excluding the first heating-cooling cycle which was used to erase the thermal history of the samples) to check reproducibility of the experiment. Data treatment was performed using the NanoAnalyze software.

Optical microscopy

The samples were prepared by mixing **C_3Pyr** (8 mg.mL^{-1}), the minimum amount of acceptor to observe gelation and TCE. These were subsequently heated till complete solubilisation and drop-casted on a glass slide. After evaporation of the solvent, micrographs were recorded with a Leica DM 2500P microscope.

SEM Microscopy

The **C_3Pyr** (32 mg.mL^{-1}) and $(A)_3/(\mathbf{C_3Pyr})_1$ gel samples were casted onto aluminium stubs and the TCE solvent left to evaporate. To facilitate SEM measurements of the texture, samples were covered in Pt and mounted onto the SEM-FEG (Hitachi SU-70) microscope operating at 5 kV.

ATR-IR spectroscopy

The vibrational spectra were acquired with a resolution of 0.5 cm^{-1} on a FT-IR Bruker Tensor 27 or a FT-IR VERTEX 70.

^{1}H-NMR spectroscopy

Spectra were measured on a Bruker Avance III nanobay 300 MHz or a Bruker Avance DRX 300 (^{1}H: 300 MHz). Spectra were calibrated according to the residual signal of TCE (6.0 ppm)

UV-visible absorption spectroscopy

Absorption spectra were recorded on an Agilent Cary Series UV-visible spectrophotometer or on Perkin Elmer Lambda 2 or 19 spectrophotometers. The variable-temperature UV-visible measurements were conducted in the range 20-100 °C. The $(A)_3/(\mathbf{C_3Pyr})_1$ in TCE samples were prepared for the concentration of 8 mg.mL-1 in a quartz cuvette of 1 mm path length.

Computational details

Calculations have been performed with the Gaussian package.[83] Geometry optimization as well as absorption spectra have been performed with the ωb97xd functional[84] in combination with the 6-31+G(d) basis set. The first 20 excited states were calculated and a gaussian broadening of 0.2 eV was applied.

Fluorescence spectroscopy

Emission spectra were recorded on a Photon Technology International QuantaMaster 4. The samples were systematically prepared in 1,1,2,2-tetrachloroethane and the temperature was controlled through a Peltier system.

Acknowledgements

This work was supported by the French Agence Nationale de la Recherche (ANR-16-CE09-0013 FOGEL project) and the Région Pays-de-la-Loire (PHOTOGEL project). M. L. thanks SeRC (Swedish e-Science Research Center) for funding. The Swedish National Infrastructure for Computing (SNIC) at National Supercomputer Centre (NSC) and Center for High Performance Computing (PDC) are acknowledged for providing computer resources. D. C. thanks the CNRS Section 12 for a *Délégation* period and the University of Angers for a *CRCT* research leave.

Keywords: Supramolecular polymers • Gels • Charge-transfer complexes • Pyrene • Spectroscopic properties

[1] P. Terech, R. G. Weiss, *Chem. Rev.* **1997**, *97*, 3133–3159.
[2] N. M. Sangeetha, U. Maitra, *Chem. Soc. Rev.* **2005**, *34*, 821–836.
[3] L. A. Estroff, A. D. Hamilton, *Chem. Rev.* **2004**, *104*, 1201–1217.
[4] B.-K. An, D.-S. Lee, J.-S. Lee, Y.-S. Park, H.-S. Song, S. Y. Park, *J. Am. Chem. Soc.* **2004**, *126*, 10232–10233.
[5] F. Camerel, L. Bonardi, M. Schmutz, R. Ziessel, *J. Am. Chem. Soc.* **2006**, *128*, 4548–4549.
[6] X. Dou, W. Pisula, J. Wu, G. J. Bodwell, K. Müllen, *Chem. - Eur. J.* **2008**, *14*, 240–249.
[7] T. Shu, J. Wu, M. Lu, L. Chen, T. Yi, F. Li, C. Huang, *J. Mater. Chem.* **2008**, *18*, 886–893.
[8] A. Ajayaghosh, V. K. Praveen, C. Vijayakumar, *Chem Soc Rev* **2008**, *37*, 109–122.

[9] H. Jintoku, M.-T. Kao, A. Del Guerzo, Y. Yoshigashima, T. Masunaga, M. Takafuji, H. Ihara, *J. Mater. Chem. C* **2015**, *3*, 5970–5975.
[10] X. Yang, Y. Liu, J. Li, Q. Wang, M. Yang, C. Li, *New J. Chem.* **2018**, *42*, 17524–17532.
[11] X. Yan, F. Wang, B. Zheng, F. Huang, *Chem. Soc. Rev.* **2012**, *41*, 6042–6065.
[12] K. K. Kartha, S. S. Babu, S. Srinivasan, A. Ajayaghosh, *J. Am. Chem. Soc.* **2012**, *134*, 4834–4841.
[13] M. D. Segarra-Maset, V. J. Nebot, J. F. Miravet, B. Escuder, *Chem. Soc. Rev.* **2013**, *42*, 7086–7098.
[14] Y. Ma, M. Cametti, Z. Džolić, S. Jiang, *J. Mater. Chem. C* **2018**, *6*, 9232–9237.
[15] N. Malviya, C. Sonkar, B. K. Kundu, S. Mukhopadhyay, *Langmuir* **2018**, *34*, 11575–11585.
[16] K. Roy, S. Ghosh, M. Chetia, P. Satpati, S. Chatterjee, *Org. Biomol. Chem.* **2019**, *17*, 3026–3039.
[17] Y. Ni, X. Li, J. Hu, S. Huang, H. Yu, *Chem. Mater.* **2019**, *31*, 3388–3394.
[18] J. Puigmarti-Luis, D. B. Amabilino, in *Funct. Mol. Gels*, The Royal Society Of Chemistry, **2014**, pp. 195–254.
[19] S. S. Babu, V. K. Praveen, A. Ajayaghosh, *Chem. Rev.* **2014**, *114*, 1973–2129.
[20] J. A. Foster, M.-O. Piepenbrock M., G. O. Lloyd, N. Clarke, J. Howard A. K., J. W. Steed, *Nat. Chem.* **2010**, *2*, 1037–1043.
[21] F. Aparicio, E. Matesanz, L. Sanchez, *Chem. Commun.* **2012**, *48*, 5757–5759.
[22] D. K. Kumar, J. W. Steed, *Chem. Soc. Rev.* **2014**, *43*, 2080–2088.
[23] C. Rizzo, R. Arrigo, F. D'Anna, F. Di Blasi, N. T. Dintcheva, G. Lazzara, F. Parisi, S. Riela, G. Spinelli, M. Massaro, *J. Mater. Chem. B* **2017**, *5*, 3217–3229.
[24] K. Sharma, J. P. Joseph, A. Sahu, N. Yadav, M. Tyagi, A. Singh, A. Pal, K. P. R. Kartha, *RSC Adv.* **2019**, *9*, 19819–19827.
[25] S. Prasanthkumar, S. Ghosh, V. C. Nair, A. Saeki, S. Seki, A. Ajayaghosh, *Angew. Chem. Int. Ed.* **2015**, *54*, 946–950.
[26] C. Giansante, G. Raffy, C. Schäfer, H. Rahma, M.-T. Kao, A. G. L. Olive, A. Del Guerzo, *J. Am. Chem. Soc.* **2011**, *133*, 316–325.
[27] J. Zheng, W. Qiao, X. Wan, J. P. Gao, Z. Y. Wang, *Chem. Mater.* **2008**, *20*, 6163–6168.
[28] S. V. Shinde, M. Kulkarni, P. Talukdar, *RSC Adv.* **2016**, *6*, 30690–30694.
[29] A. Sarkar, S. Dhiman, A. Chalishazar, S. J. George, *Angew. Chem. Int. Ed.* **2017**, *56*, 13767–13771.
[30] Q. Chen, D. Zhang, G. Zhang, X. Yang, Y. Feng, Q. Fan, D. Zhu, *Adv. Funct. Mater.* **2010**, *20*, 3244–3251.
[31] H. Wu, L. Xue, Y. Shi, Y. Chen, X. Li, *Langmuir* **2011**, *27*, 3074–3082.
[32] M. Wehner, M. I. S. Röhr, M. Bühler, V. Stepanenko, W. Wagner, F. Würthner, *J. Am. Chem. Soc.* **2019**, *141*, 6092–6107.
[33] X. Sui, X. Feng, M. A. Hempenius, G. J. Vancso, *J. Mater. Chem. B* **2013**, *1*, 1658.
[34] M. Kumar, K. Venkata Rao, S. J. George, *Phys Chem Chem Phys* **2014**, *16*, 1300–1313.
[35] F. M. Winnik, *Chem. Rev.* **1993**, *93*, 587–614.
[36] V. D. Parker, *J. Am. Chem. Soc.* **1976**, *98*, 98–103.
[37] P. Babu, N. M. Sangeetha, P. Vijaykumar, U. Maitra, K. Rissanen, A. R. Raju, *Chem. – Eur. J.* **2003**, *9*, 1922–1932.
[38] A. Pal, S. Karthikeyan, R. P. Sijbesma, *J. Am. Chem. Soc.* **2010**, *132*, 7842–7843.
[39] J. R. Moffat, D. K. Smith, *Chem. Commun.* **2011**, *47*, 11864–11866.
[40] X.-D. Xu, J. Zhang, X. Yu, L.-J. Chen, D.-X. Wang, T. Yi, F. Li, H.-B. Yang, *Chem. - Eur. J.* **2012**, *18*, 16000–16013.
[41] J. A. Foster, R. M. Edkins, G. J. Cameron, N. Colgin, K. Fucke, S. Ridgeway, A. G. Crawford, T. B. Marder, A. Beeby, S. L. Cobb, J. W. Steed, *Chem. – Eur. J.* **2014**, *20*, 279–291.
[42] N. Chebotareva, P. H. H. Bomans, P. M. Frederik, N. A. J. M. Sommerdijk, R. P. Sijbesma, *Chem. Commun.* **2005**, 4967–4969.
[43] S. Roy, A. Baral, A. Banerjee, *Chem. – Eur. J.* **2013**, *19*, 14950–14957.
[44] P. Rajamalli, E. Prasad, *Soft Matter* **2012**, *8*, 8896.
[45] L. Zhang, C. Liu, Q. Jin, X. Zhu, M. Liu, *Soft Matter* **2013**, *9*, 7966.
[46] T.-L. Lai, D. Canevet, N. Avarvari, M. Sallé, *Chem. – Asian J.* **2016**, *11*, 81–85.
[47] U. Maitra, P. V. Kumar, N. Chandra, L. J. D'Souza, M. D. Prasanna, A. R. Raju, *Chem. Commun.* **1999**, 595–596.
[48] J. Hu, J. Wu, Q. Wang, Y. Ju, *Beilstein J. Org. Chem.* **2013**, *9*, 2877–2885.
[49] A. Hahma, S. Bhat, K. Leivo, J. Linnanto, M. Lahtinen, K. Rissanen, *New J. Chem.* **2008**, *32*, 1438–1448.
[50] J. R. Moffat, D. K. Smith, *Chem. Commun.* **2008**, 2248.
[51] K. Miyamoto, H. Jintoku, T. Sawada, M. Takafuji, T. Sagawa, H. Ihara, *Tetrahedron Lett.* **2011**, *52*, 4030–4035.
[52] C.-B. Huang, L.-J. Chen, J. Huang, L. Xu, *RSC Adv.* **2014**, *4*, 19538–19549.
[53] B. Adhikari, J. Nanda, A. Banerjee, *Chem. – Eur. J.* **2011**, *17*, 11488–11496.
[54] S. Cantekin, T. F. A. de Greef, A. R. A. Palmans, *Chem. Soc. Rev.* **2012**, *41*, 6125.
[55] A. R. A. Palmans, J. A. J. M. Vekemans, E. E. Havinga, E. W. Meijer, *Angew. Chem. Int. Ed. Engl.* **1997**, *36*, 2648–2651.
[56] A. R. A. Palmans, J. A. J. M. Vekemans, H. Fischer, R. A. Hikmet, E. W. Meijer, *Chem. – Eur. J.* **1997**, *3*, 300–307.
[57] J. J. van Gorp, J. A. J. M. Vekemans, E. W. Meijer, *J. Am. Chem. Soc.* **2002**, *124*, 14759–14769.
[58] I. Dánilá, F. Riobé, J. Puigmartí-Luis, Á. Pérez Del Pino, J. D. Wallis, D. B. Amabilino, N. Avarvari, *J. Mater. Chem.* **2009**, *19*, 4495–4504.
[59] I. Danila, F. Riobé, F. Piron, J. Puigmartí-Luis, J. D. Wallis, M. Linares, H. Ågren, D. Beljonne, D. B. Amabilino, N. Avarvari, *J. Am. Chem. Soc.* **2011**, *133*, 8344–8353.
[60] I. Danila, F. Pop, C. Escudero, L. N. Feldborg, J. Puigmarti-Luis, F. Riobe, N. Avarvari, D. B. Amabilino, *Chem. Commun.* **2012**, *48*, 4552–4554.
[61] F. Pop, C. Melan, I. Danila, M. Linares, D. Beljonne, D. B. Amabilino, N. Avarvari, *Chem. - Eur. J.* **2014**, *20*, 17443–17453.
[62] S. Vela, J. A. Berrocal, C. Atienza, E. W. Meijer, N. Martín, *Chem. Commun.* **2017**, *53*, 4084–4087.
[63] C. Oliveras-González, M. Linares, D. B. Amabilino, N. Avarvari, *ACS Omega* **2019**, *4*, 10108–10120.
[64] T.-L. Lai, F. Pop, C. Melan, D. Canevet, M. Sallé, N. Avarvari, *Chem. – Eur. J.* **2016**, *22*, 5839–5843.
[65] The critical gelation concentration is defined as the minimum concentration for which the inverted sample resists flow, 24 hours after cooling the hot solution.
[66] A. Sandeep, V. K. Praveen, K. K. Kartha, V. Karunakaran, A. Ajayaghosh, *Chem. Sci.* **2016**, *7*, 4460–4467.
[67] J. A. Dean, *Lange's Handbook of Chemistry***.**
[68] A. Nagai, J. B. Miller, J. Du, P. Kos, M. C. Stefan, D. J. Siegwart, *Chem. Commun.* **2015**, *51*, 11868–11871.
[69] R. J. Dillon, C. J. Bardeen, *J. Phys. Chem. A* **2012**, *116*, 5145–5150.
[70] P. Terech, C. Rossat, F. Volino, *J. Colloid Interface Sci.* **2000**, *227*, 363–370.
[71] S. Bhattacharjee, S. Bhattacharya, *Chem. – Asian J.* **2015**, *10*, 572–580.
[72] S. Bhattacharjee, B. Maiti, S. Bhattacharya, *Nanoscale* **2016**, *8*, 11224–11233.
[73] T. F. A. De Greef, M. M. J. Smulders, M. Wolffs, A. P. H. J. Schenning, R. P. Sijbesma, E. W. Meijer, *Chem. Rev.* **2009**, *109*, 5687–5754.
[74] J. S. Chappell, A. N. Bloch, W. A. Bryden, M. Maxfield, T. O. Poehler, D. O. Cowan, *J. Am. Chem. Soc.* **1981**, *103*, 2442–2443.
[75] L. Kaboub, S. Fradj, A. Gouasmia, *Molecules* **2006**, *11*, 776–785.
[76] M. Meneghetti, C. Pecile, *J. Chem. Phys.* **1986**, *84*, 4149–4162.
[77] H. Jiang, P. Hu, J. Ye, K. K. Zhang, Y. Long, W. Hu, C. Kloc, *J. Mater. Chem. C* **2018**, *6*, 1884–1902.
[78] P. Hu, H. Li, Y. Li, H. Jiang, C. Kloc, *CrystEngComm* **2017**, *19*, 618–624.
[79] A. Salmerón-Valverde, S. Bernès, *CrystEngComm* **2015**, *17*, 6227–6235.
[80] M. A. Dobrowolski, G. Garbarino, M. Mezouar, A. Ciesielski, M. K. Cyrański, *CrystEngComm* **2014**, *16*, 415–429.
[81] R. L. Martin, *J. Chem. Phys.* **2003**, *118*, 4775–4777.
[82] S. A. Boer, R. P. Cox, M. J. Beards, H. Wang, W. A. Donald, T. D. M. Bell, D. R. Turner, *Chem. Commun.* **2019**, *55*, 663–666.
[83] M. J. Frisch *et al.*, *Gaussian 16 Rev. C.01*, Wallingford, CT, **2016**.
[84] J.-D. Chai, M. Head-Gordon, *Phys. Chem. Chem. Phys.* **2008**, *10*, 6615.

Entry for the Table of Contents

FULL PAPER

Organogels were formed from a C_3-symmetric gelator through charge-transfer complexation. Their properties proved to be highly dependent on the nature of the electron poor dopant. The latter significantly influenced the gelation domains, the gel-to-sol transition temperatures, the microstructures formed in the xerogel state as well as their spectroscopic properties (absorption and emission).

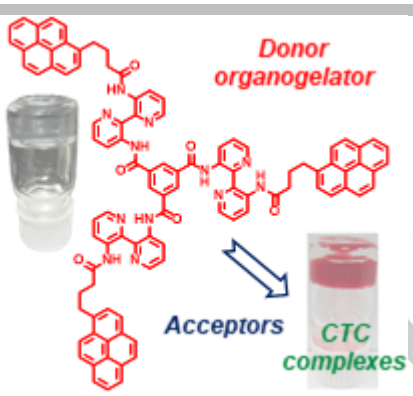

Adrian Gainar, Thanh-Loan Lai, Cristina Oliveras, Flavia Pop, Matthieu Raynal, Benjamin Isare, Laurent Bouteiller, Mathieu Linares, David Canevet,* Narcis Avarvari,* Marc Sallé**

Page No. – Page No.

Tuning the organogelating and spectroscopic properties of a C_3-symmetric pyrene-based gelator through charge transfer